Design and Experiment on Differentially-Driven Microstrip Antennas

Yue Ping Zhang

***Abstract*—Design and experiment is given of differentially-driven microstrip antennas. First, the design formulas to determine the patch dimensions and the location of the feed point for single-ended microstrip antennas are examined to design differentially-driven microstrip antennas. It is found that the patch length can still be designed using the formulas for the required resonant frequency but the patch width calculated by the formula usually needs to be widen to ensure the excitation of the fundamental mode using the probe feeds. The condition that links the patch width, the locations of the probe feeds, and the excitation of the fundamental mode is given. Second, the wideband techniques for single-ended microstrip antennas are evaluated for differentially-driven microstrip antennas. A novel H-slot is proposed for differentially-driven microstrip antennas to improve impedance bandwidth. Third, the effects of imperfect differential signal conditions on the performance of differentially-driven microstrip antennas are investigated for the first time. It is found that they only degrade the polarization purity in the H-plane with an increased radiation of cross-polarization. Finally, both differentially-driven and single-ended microstrip antennas were fabricated and measured. It is shown that the simulated and measured results are in acceptable agreement. More importantly, it is also shown that the differentially-driven microstrip antenna has wider impedance bandwidth of measured 4.1% and simulated 3.9% and higher gain of measured 4.2 dBi and simulated 3.7 dBi as compared with those of measured 1.9% and simulated 1.3% and gain of measured 1.2 dBi and simulated 1.2 dBi of the single-ended microstrip antenna.**

***Index Terms*—Cavity model, input impedance, microstrip patch antenna, radiation pattern.**

I. Introduction

MICROSTRIP antennas have many unique and attractive properties – low in profile, light in weight, compact and conformable in structure, and easy to fabricate and to be integrated with solid-state devices [1]. Therefore, they have been widely used in radio systems for various applications. Radio systems have been traditionally designed for single-ended signal operation, so have been microstrip antennas. Recently, radio systems have begun to be designed for differential signal operation [2]. This is because the differential signal operation is more suitable for high-level integration or single-chip solution of radio systems. Radio systems that adopt differential signal operation require differential antennas to get rid of bulky off-chip and lossy on-chip balun to improve the receiver noise performance and transmitter power efficiency [3]. There have been a few papers about differential microstrip antennas [4]–[8]. They focus on either integration with solid-state circuits or analysis of differential signal operation and indeed provide little information on the design of differential microstrip antennas. In this paper we present the design and experiment on differentially-driven microstrip antennas. We examine the applicability of the design formula and the wideband techniques of single-ended microstrip antennas for differentially-driven microstrip antennas in Section II. We also evaluate the effects of imperfect differential signal conditions on the performance of differentially-driven microstrip antennas in this Section. We describe the experiment and discuss the measured results to validate the designs in Section III. Finally, we summarize the conclusions in Section IV.

Manuscript received July 12, 2006; revised December 30, 2006.

The author is with the Integrated Systems Research Lab, School of Electrical and Electronic Engineering, Nanyang Technological University, Singapore 639798, Singapore (e-mail: eypzhang@ntu.edu.sg).

Color versions of one or more of the figures in this paper are available online at http://ieeexplore.ieee.org.

Digital Object Identifier 10.1109/TAP.2007.905832

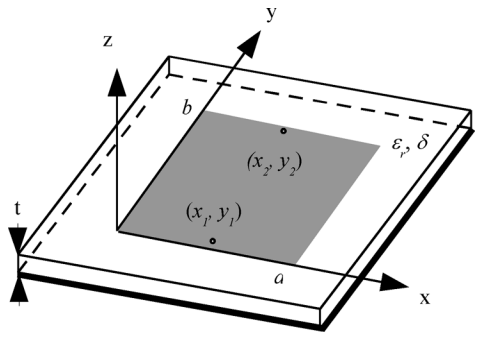

Fig. 1. Differentially-driven microstrip antenna.

II. Design of Differentially-Driven Microstrip Antennas

A microstrip antenna and a coordinate system are illustrated in Fig. 1. The microstrip antenna that has the patch width a along x-axis and the patch length b along y-axis located on the surface of a grounded dielectric substrate with thickness t, dielectric constant ε_r, and dielectric loss tangent δ is differentially driven at points (x_1, y_1) and (x_2, y_2). The design of the differentially-driven microstrip antenna is to determine the patch width a and length b and the driving points (x_1, y_1) and (x_2, y_2) necessary to satisfy the input impedance and radiation characteristics with the given information on the substrate.

The input impedance Z_d of the differentially-driven microstrip antenna is given by [8]

$$Z_d = 2(Z_{11} - Z_{21}) = 2(Z_{22} - Z_{12}) \tag{1}$$

where the Z parameters are defined at the driving points (x_1, y_1) and (x_2, y_2) and they can be easily calculated with the improved

cavity model [9]. Equation (1) reveals that there is a cancellation mechanism, which may improve the impedance bandwidth. The value of Z_d is required in the design of matching network between the differentially-driven microstrip antenna and the differential active circuitry in a radio system. The S_{11} calculated from Z_d is given by

$$S_{11} = \frac{Z_d - Z_c}{Z_d + Z_c} \tag{2}$$

where Z_c is 100 Ω.

The radiation of the differentially-driven microstrip antenna also originates from two slots and each slot can be thought of as radiating the same field as a magnetic dipole with a magnetic current. The magnetic current is directly proportional to the z component of electric field in the cavity region, which can be written as in (3) at the bottom of the page, where α and θ represent the amplitude and phase imbalance at the two driving points, respectively, and all others have their usual meaning [8]. Ideally, $\alpha = 0$ and $\theta = 0^\circ$, thus it can be seen from (3) that the differentially-driven microstrip antenna introduces the cancellation mechanism, which can be explored to suppress some higher-order modes to reduce the cross polarization radiation. Practically, α can be up to 0.1 (1 dB) and θ to 10°, the effects of such imperfect differentially-driven conditions on the performance of the differentially-driven microstrip antenna are not clear and worthwhile investigating.

A. Design Procedure

For a single-ended microstrip antenna, the patch width a and length b that support the operation at the required resonant frequency (or the free-space wavelength λ_o) can be designed using the formulas as given in [10] as

$$a = \frac{\lambda_o}{2\sqrt{\frac{\varepsilon_r+1}{2}}} \tag{4}$$

$$b = \frac{\lambda_o}{2\sqrt{\varepsilon_e}} - 2\Delta b \tag{5}$$

where

$$\Delta b = 0.412t\frac{(\varepsilon_e + 0.3)\left(\frac{a}{t} + 0.264\right)}{(\varepsilon_e - 0.258)\left(\frac{a}{t} + 0.8\right)} \tag{6}$$

$$\varepsilon_e = \frac{\varepsilon_r + 1}{2} + \frac{\varepsilon_r - 1}{2\sqrt{1 + 12\frac{t}{a}}}. \tag{7}$$

The location of the driving point at (x_1, y_1) for matching to 50 Ω can be determined as

$$x_1 = \frac{a}{2} \tag{8}$$

$$y_1 = \frac{b}{\pi}\cos^{-1}\frac{a\sqrt{5(\varepsilon_r - 1)}}{3\varepsilon_r b} \tag{9}$$

where $0 \le y_1 < b/2$ [11].

While for a differentially-driven microstrip antenna, it is found that the patch length b can still be designed using formulas (4) to (9) for the required resonant frequency. However, the patch width a calculated by formula (4) usually needs to be widen to ensure the excitation of the fundamental mode TM_{01} using the probe feeds. It is known that the larger the patch width is, the higher the radiation efficiency is. The limiting factor for the patch width is the undesirable influence of higher-order modes. For the differentially-driven microstrip antenna, higher-order modes are significantly suppressed. Hence, the patch width for the differentially-driven microstrip antenna can be much larger than that of the single-ended counterpart. The appropriate patch width a for practical use can be determined together with the location of the driving point (x_2, y_2) for the differentially-driven microstrip antenna. It is natural to locate the driving point (x_2, y_2) at the mirror point of (x_1, y_1) along the line $x = a/2$ within the patch. The condition for the excitation of the fundamental mode TM_{01} using the probe feeds depends on the ratio of the separation to the free-space wavelength, which is given in [8] as

$$\frac{\xi}{\lambda_o} = \frac{y_2 - y_1}{\lambda_o} \ge 0.1 \tag{10}$$

for an electrically thin substrate of low permittivity. Thus, the patch width for the differentially-driven microstrip antenna can be determined by widening the width calculated from formula (4) to that at which the condition (10) is satisfied.

Design using formulas (4) to (10) on the FR4 substrate with $t = 1.6$ mm, $\varepsilon_r = 4.4$, and $\delta = 0.025$ at 2 GHz yields $a = 74.4$ mm, $b = 35$ mm, $(x_1, y_1) = (a/2, 9.654\ \mathrm{mm})$, and $(x_2, y_2) = (a/2, 25.346\ \mathrm{mm})$ for the differentially-driven microstrip antenna. The condition $\xi/\lambda_o = 15.692/150 = 0.105 > 0.1$ is satisfied. Simulations using the HFSS were made for the microstrip antennas with a square substrate and ground plane of size $\lambda_o \times \lambda_o$. Fig. 2 shows the simulated input impedances of the microstrip antennas driven at (x_1, y_1) and (x_2, y_2) for differential signal operation and driven at (x_1, y_1) for single-ended signal operation as well. The impedance characteristics give insight on how an antenna must be modified to achieve a specified resonant frequency. Here, the resonant frequency is defined as where the reactance of the input impedance is equal to zero. According to this definition, one can see that the simulated resonant frequencies are at 1.93 GHz for the differentially-driven microstrip antenna and at 1.91 GHz for the single-ended microstrip antenna. The errors in predicting resonant frequencies between the calculations and simulations are 3.5% and 4.5% for the differentially-driven and single-ended microstrip antennas, respectively. The higher resonant frequency of the differentially-driven microstrip antenna could be due to the reactive cancellation between the inductance and capacitance introduced by the two feeds. Fig. 3 shows the

$$E_z = j\mu_o \sum_{m,n=0}^{\infty} \frac{\phi_{mn}(x,y)}{k_e^2 - k_{mn}^2} j_o\left(\frac{m\pi d_e}{2a_e}\right) I\left[\phi_{mn}(x_1,y_1) - (1-\alpha)\,\phi_{mn}(x_2,y_2)\cos\theta\right] \tag{3}$$

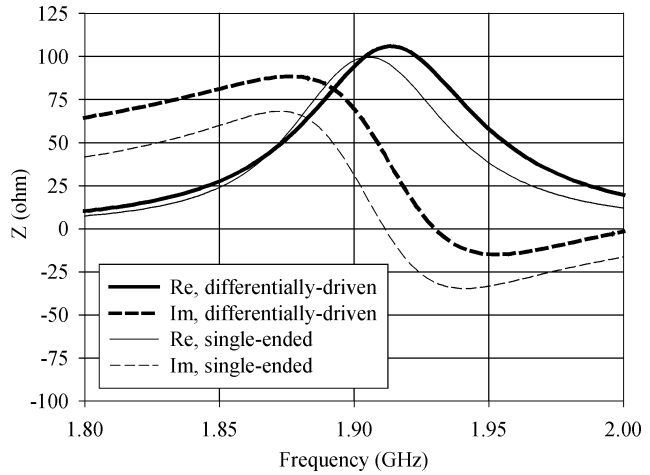

Fig. 2. Input impedance of the differentially-driven and single-ended microstrip antennas.

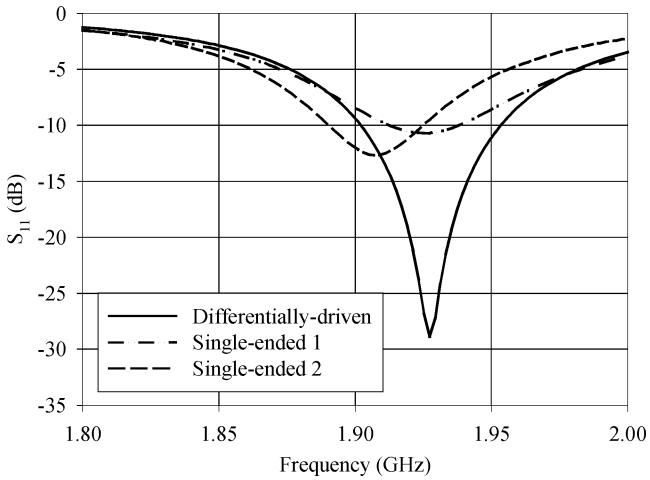

Fig. 3. S_{11} of the differentially-driven and single-ended microstrip antennas.

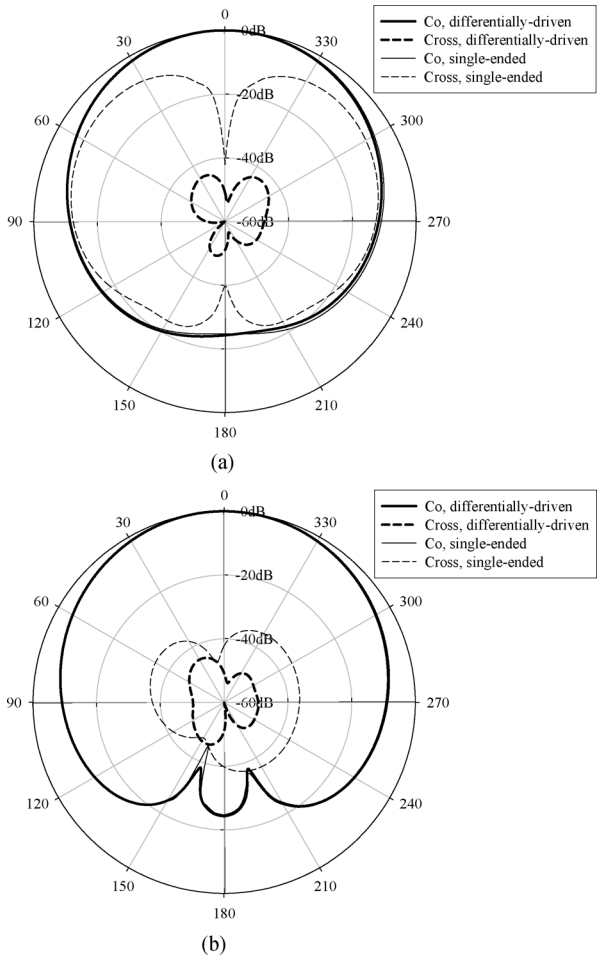

Fig. 4. Radiation patterns of the differentially-driven and single-ended microstrip antennas: (a) in the H-plane and (b) in the E-plane where solid and dashed lines represent the radiation of co- and cross-polarization, respectively.

simulated S_{11} corresponding to the differentially-driven and single-ended microstrip antennas. The S_{11} indicates how well the antenna is matched to a signal source and how wide the impedance bandwidth is. The impedance bandwidth is the difference between the upper and lower frequencies for which the S_{11} is less than or equal to -9.5 dB (or VSWR less than or equal to 2). The percentage bandwidth is defined here as the difference between the upper and lower frequencies for which the S_{11} is less than or equal to -9.5 dB divided by the average of the upper and lower frequencies. The simulated impedance bandwidths are 50 MHz ($50/1925 = 2.6\%$) and 35 MHz ($35/1925 = 1.8\%$) for the differentially-driven and single-ended microstrip antennas, respectively. It is found that the simulated impedance bandwidth 1.8% for the single-ended microstrip antenna is quite close to 1.5% calculated from the simple empirical formula given by

$$B = 3.77\frac{\varepsilon_r - 1}{\varepsilon_r^2}\frac{a}{b}\frac{t}{\lambda_o} \tag{11}$$

where $t \ll \lambda_o$ [11]. An effort has also been made to improve the matching for the single-ended microstrip antenna by moving the driving point. It is shown in Fig. 3 as the case of single-ended 2 the matching is improved and so is the impedance bandwidth ($40/1912 = 2.09\%$) when the driving point is located at $(x_1, y_1) = (a/2, 15.654\,\text{mm})$. The wider impedance bandwidth of the differentially-driven microstrip antenna (2.6%) than that of the single-ended microstrip antenna (1.8% or 2.09%) is the result of reactive cancellation between the capacitance and inductance introduced by the two probe feeds of the differentially-driven microstrip antenna. Fig. 4 shows the simulated radiation patterns of the microstrip antenna driven for differential and single-ended signal operations at their respective resonant frequencies. As expected, the radiation of cross-polarization from the differentially-driven microstrip antenna is much weaker than that of the single-ended microstrip antenna. In addition, the simulations show that the gain of the differentially-driven microstrip antenna is 3.72 dBi, which is much higher than that 1.2 dBi of the single-ended microstrip antenna.

Simulations using the HFSS were also made for the differentially-driven microstrip antenna with a square substrate and ground plane of size $\lambda_o/2 \times \lambda_o/2$ to investigate the influences of the ground plane on the resonant frequency, impedance bandwidth, and radiation pattern of the differentially-driven microstrip antenna. The simulated results show

that the size reduction of the ground plane from one- to half-wavelength increases the resonant frequency to 1.958 GHz from 1.93 GHz, reduces the impedance bandwidth to 47 MHz ($47/1934 = 2.4\%$) from 50 MHz ($50/1925 = 2.6\%$), and greatly enhances the radiation of cross-polarization.

B. Wideband Techniques

Single-ended microstrip antennas have narrow impedance bandwidth, so do differentially-driven microstrip antennas. Some useful wideband techniques have been devised for single-ended microstrip antennas in addition to the common methods of increasing substrate thickness and deceasing substrate permittivity [10]. These include using impedance matching, optimized patch geometry, multiple resonances, etc. We will see that the direct application of these techniques to differentially-driven microstrip antennas will have some problems. For example, the impedance-matching approach will significantly increase the size of a differentially-driven microstrip antenna because the matching networks are needed at both feeds. The technique of the optimized patch geometry using the generic algorithm will result in a very irregular and unconventional patch shape that is difficult to fabricate and to maintain the structural symmetry for the efficient radiation of differential signal. The multiple-resonance technique relies on adding parasitic patches, cutting slots, etc. Parasitic patches can be added in either planar or stacked configurations. Adding parasitic patches in planar configuration must maintain the structural symmetry for the efficient radiation of differential signal; as a result, it is very likely that the differentially-driven microstrip antenna appears much bulkier than its single-ended-driven counterpart. While adding a parasitic patch in stacked configuration increases the thickness of the differentially-driven microstrip antenna but can naturally maintain the structural symmetry for the efficient radiation of differential signal and also can keep the differentially-driven microstrip antenna as compact as its single-ended-driven counterpart. Hence, the multiple-resonance technique by a stacked parasitic patch is more appropriate than that by planar parasitic patches to a differentially-driven microstrip antenna for the impedance bandwidth enhancement.

Slots can be cut in the patch or the ground plane to improve impedance bandwidth and to reduce antenna size. A U-slot in the patch greatly improves the impedance bandwidth of a single-ended microstrip antenna. [12]. Design rules for the U-slot single-ended microstrip antennas were derived in [13], which states that there is a lower limit on the substrate thickness below which wideband operation is unlikely. Considering that the dual feeds are required for a differentially-driven microstrip antenna, a novel H-slot is proposed, which is shown in Fig. 5.

As an example, a single-layer H-slot differentially-driven microstrip antenna is designed on the substrate with $t = 6.35\ \mathrm{mm}$, $\varepsilon_r = 2.2$. The substrate thickness and permittivity of the H-slot differentially-driven microstrip antenna are selected and satisfied the rule of thumb for the U-slot single-ended microstrip antenna at 2.15 GHz [13]. The design yields the patch dimensions $a = 74\ \mathrm{mm}$ and $b = 42\ \mathrm{mm}$ and the locations of feed points $(x_1, y_1) = (a/2, 12\ \mathrm{mm})$ and $(x_2, y_2) = (a/2, 30\ \mathrm{mm})$ for the H-shaped slot differentially-driven microstrip antenna. The horizontal slot is 1 mm wide and 16 mm long cut with its middle point at $x = a/2$ and $y = b/2$. Both vertical slots are 3 mm wide and 34 mm long. The left vertical slot is cut with its middle point at $x = 66.5\ \mathrm{mm}$ and $y = b/2$ and the right vertical slot is cut with its middle point at $x = 83.5\ \mathrm{mm}$ and $y = b/2$, respectively.

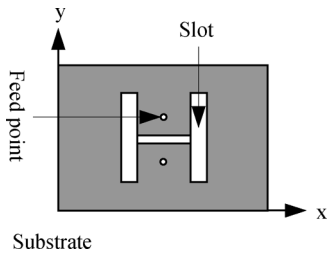

Fig. 5. A novel H-slot for differentially-driven microstrip antennas.

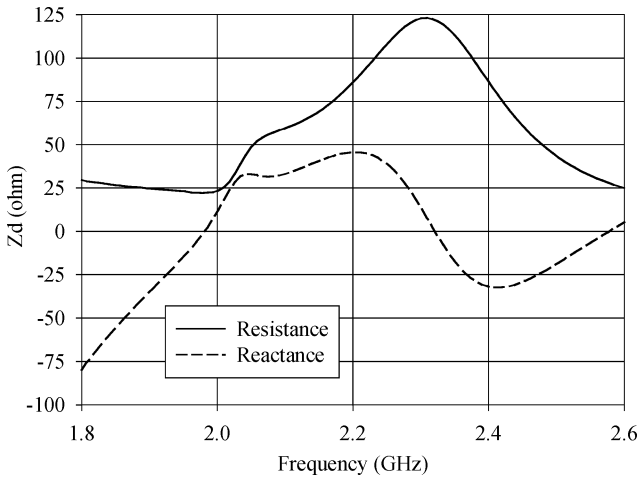

Fig. 6. Input impedance of the H-slot differentially-driven microstrip antenna.

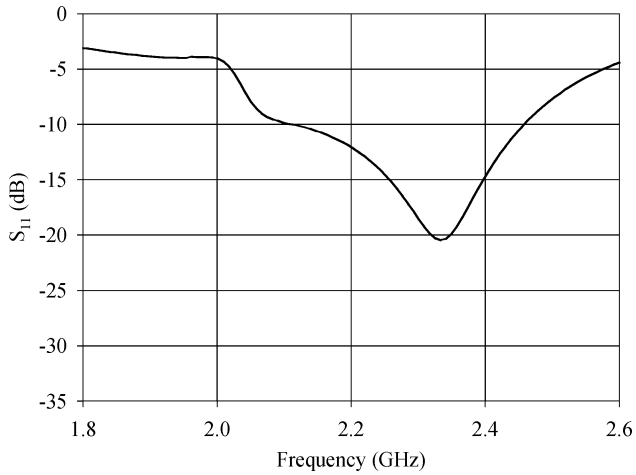

Fig. 7. S_{11} of the H-slot differentially-driven microstrip antenna.

Fig. 6 shows the simulated input impedance of the H-slot differentially-driven microstrip antenna. It is noted that the multiple resonances occur at 1.95, 2.35, and 2.58 GHz, respectively. It should be mentioned that no resonance occurs if there is no H-slot. Fig. 7 shows the simulated S_{11} of the H-slot differentially-driven microstrip antenna. The simulated impedance bandwidth is 360 MHz ($360/2260 = 16\%$). The reason for

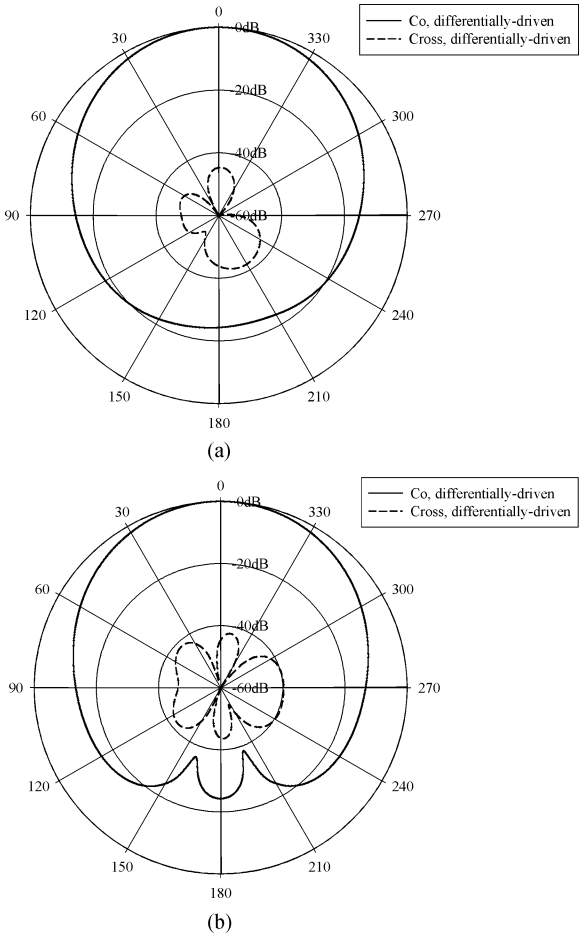

Fig. 8. Radiation patterns of the H-slot differentially-driven microstrip antenna: (a) in the H-plane, (b) in the E-plane where solid and dashed lines represent the radiation of co- and cross-polarization, respectively.

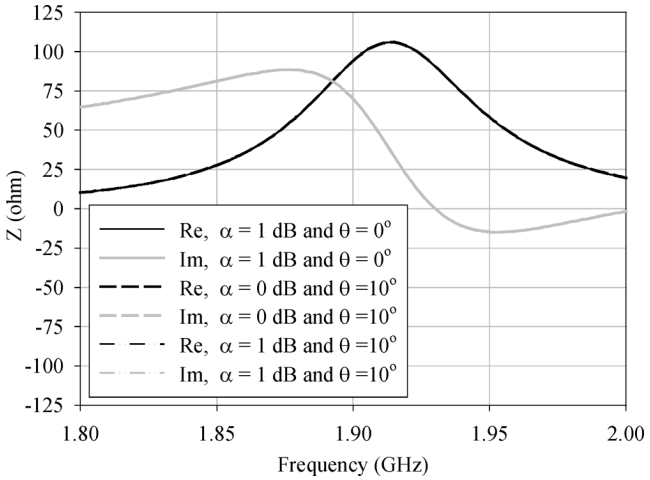

Fig. 9. Input impedance versus frequency of the differentially-driven microstrip antenna for ($\alpha = 1$ dB and $\theta = 0°$), ($\alpha = 0$ dB and $\theta = 10°$), and ($\alpha = 1$ dB and $\theta = 10°$), respectively.

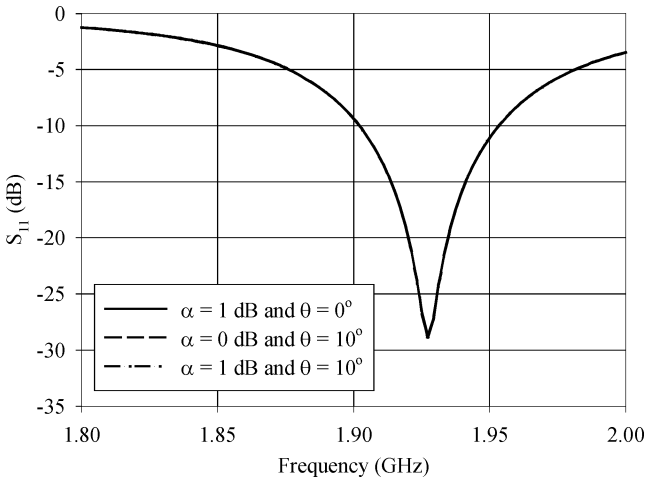

Fig. 10. S_{11} of the differentially-driven microstrip antenna for ($\alpha = 1$ dB and $\theta = 0°$), ($\alpha = 0$ dB and $\theta = 10°$), and ($\alpha = 1$ dB and $\theta = 10°$), respectively.

the broadband characteristics of the H-slot differentially-driven microstrip antenna is the same as the U-slot for the single-ended microstrip antenna. It is the result of reactive cancellation between the capacitive H-slot and the inductive probe feed and/or the currents around the H-slot [12]. Fig. 8 shows the simulated radiation patterns of the H-slot differentially-driven microstrip antenna. The radiation of cross-polarization is still much weaker than the radiation of co-polarization in both E- and H-planes. The simulated gain of the H-slot differentially-driven microstrip antenna is 7.5 dBi.

C. Effects of Imperfect Differential Signal Conditions

It is difficult to generate an ideal differential signal. Practically, the differential signal has an amplitude imbalance and a phase difference. The amplitude imbalance can be up to 1 dB and the phase difference up to 10°, respectively. The effects of such imperfect differential signal conditions on the performance of the differentially-driven microstrip antenna are simulated. Figs. 9–11 show the simulated results. As compared with the perfect differential signal condition, the imperfect differential signal conditions do not affect the input impedance, which is expected as the input impedance is independent of the signal source. However, they degrade the polarization purity in the H-plane. The degradation by the phase imbalance 10° is more severe than that by the amplitude imbalance 1 dB. The degradation of polarization purity in the H-plane can be understood from (3). The imperfect differential signal conditions decrease the cancellation extent. The higher-order modes, in particular, the TM_{20} mode can not be sufficiently suppressed; consequently, the polarization purity in the H-plane is degraded. In addition, the imperfect differential signal conditions do not alter the radiation mechanism of the microstrip antenna, the shapes of radiation patterns, especially in the E-plane, are therefore not changed.

III. Experiment on Differentially-Driven Microstrip Antennas

Both differentially-driven and single-ended microstrip antennas were constructed on the FR4 substrate for operating at 2 GHz. They had the same patch dimensions with nominal values $a = 74.4$ mm and $b = 35$ mm on the ground plane of size 150 mm × 150 mm. The driving points were located at $(x_1, y_1) = (a/2, 9.654$ mm), and

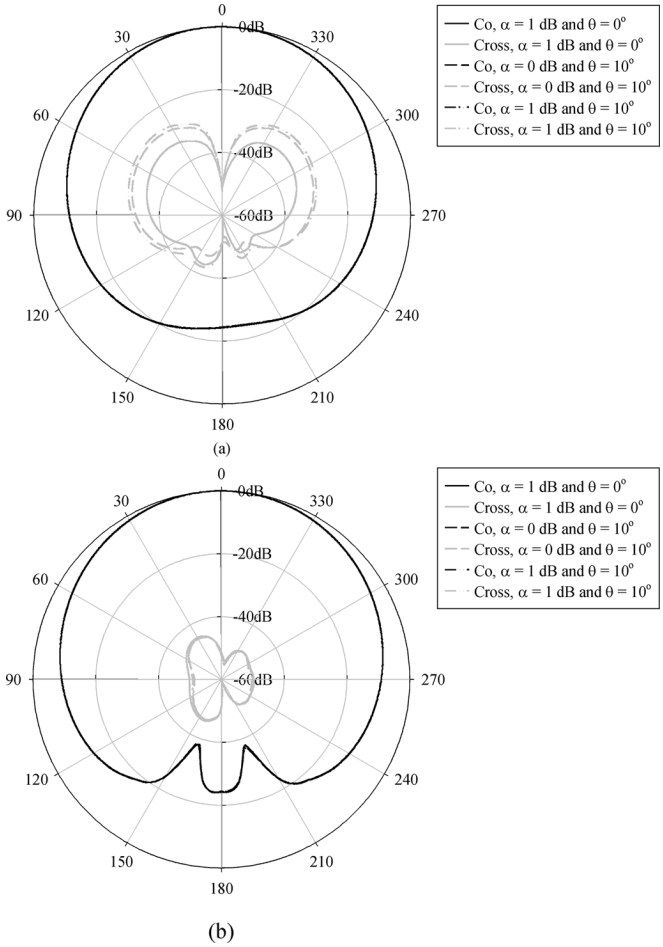

Fig. 11. Radiation patterns of the differentially-driven microstrip antenna: (a) in the H-plane and (b) in the E-plane for ($\alpha = 1$ dB and $\theta = 0°$), ($\alpha = 0$ dB and $\theta = 10°$), and ($\alpha = 1$ dB and $\theta = 10°$), respectively.

$(x_2, y_2) = (a/2, 25.346 \text{ mm})$ for the differentially-driven microstrip antenna and at $(x_1, y_1) = (a/2, 9.654 \text{ mm})$ for the single-ended microstrip antenna. An Agilent network analyzer E5062A was used to measure the S_{11}, an HP 8510C network analyzer the radiation patterns, and an Agilent signal generator 8048D and an HP spectrum analyzer 8595E the gain in an NTU anechoic chamber. Due to the lack of facilities to truly measure a differentially-driven antenna, the differentially-driven antenna is conventionally measured by using a balun that forces opposite currents in each feed of the antenna. One balun was used for the pattern and two for the gain measurements. The baluns were ZAPDJ-2 from Mini-Circuits. Fig. 12 shows the photo of the differentially-driven microstrip antenna connected with the balun and the single-ended microstrip antenna as well.

Fig. 13 shows the measured S_{11} of the balun with the two balanced ports connected though the cables to 50-Ω loads over the frequency range from 1.9 to 2.1 GHz. It is seen that S_{11} values are smaller than -10 dB over the frequency range. The amplitude imbalance and phase difference of the balun are illustrated in Fig. 14. Note that the amplitude imbalance is 0.45 dB and the phase difference is 6.8° between the 2-GHz signals at the two balanced ports.

The post simulations were made, which considered the fabrication tolerance and the measured balun performance.

Fig. 12. Photo of the differentially-driven and single-ended microstrip antennas.

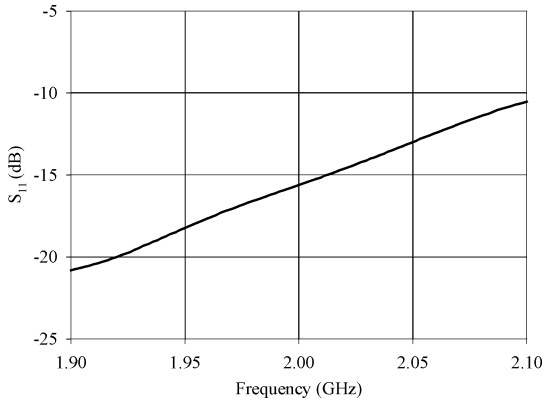

Fig. 13. Measured S_{11} of the balun.

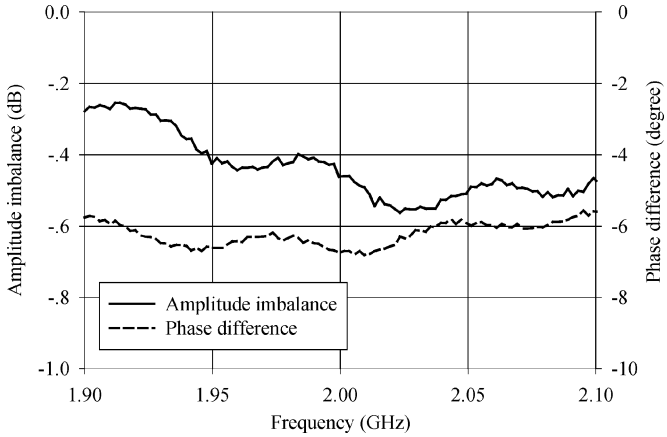

Fig. 14. Measured amplitude imbalance and phase difference of the balun.

Fig. 15 shows the simulated and measured S_{11} values of both differentially-driven and single-ended microstrip antennas. It is seen that the differentially-driven microstrip antenna has wider impedance bandwidth of measured 81.5 MHz (4.1%) and simulated 77.6 MHz (3.9%) than those of measured 37.8 MHz (1.9%) and simulated 25.8 MHz (1.3%) of the single-ended microstrip antenna. The agreement between the calculated and measured results is in general acceptable. The discrepancy is likely due to soldering and warpage and the experimental error of our measuring system.

Fig. 16 shows the simulated and measured radiation patterns of both differentially-driven and single-ended microstrip antennas at 2 GHz. It is observed that a good agreement is obtained

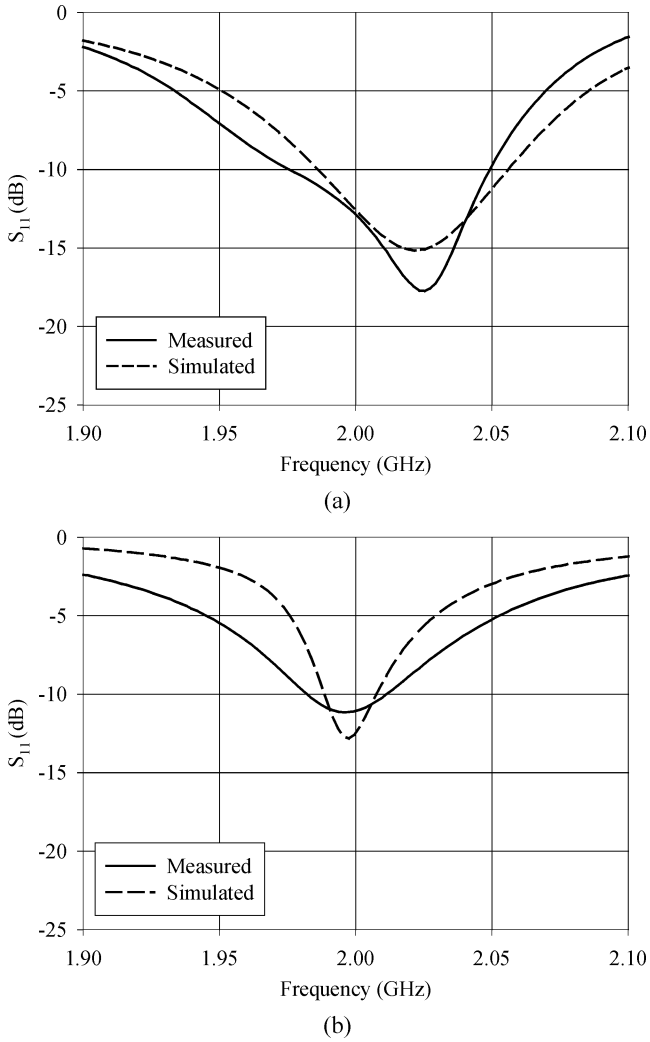

Fig. 15. Simulated and measured S_{11} versus frequency: (a) the differentially-driven antenna and (b) the single-ended microstrip antenna.

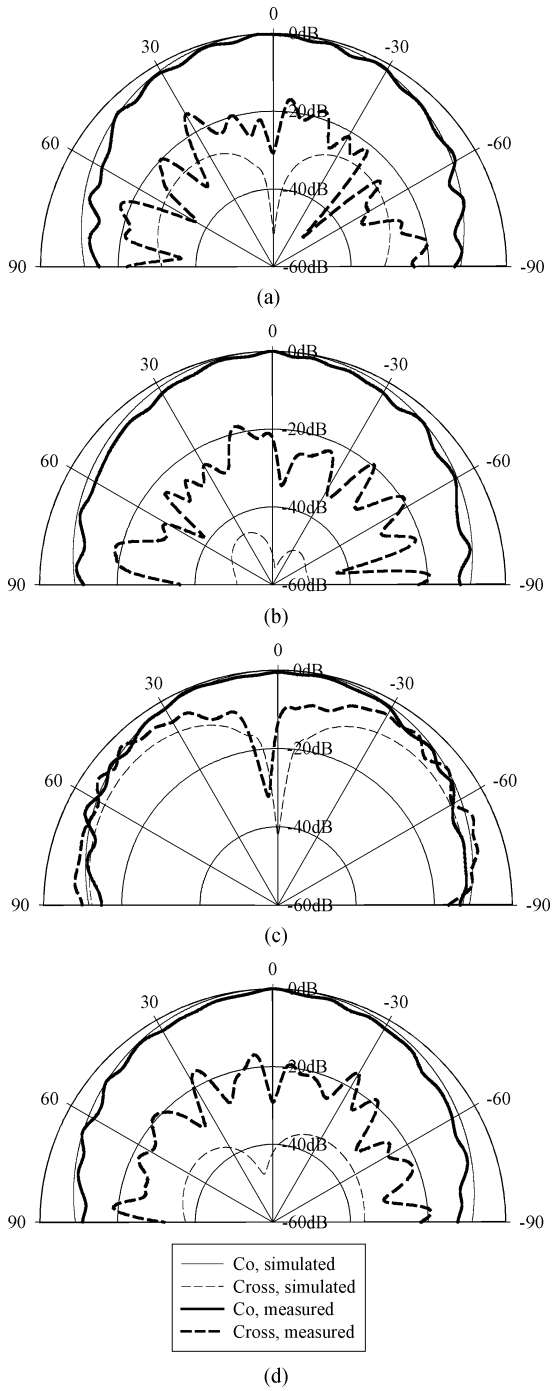

Fig. 16. Simulated and measured radiation patterns at 2.0 GHz: (a) H-plane, (b) E-plane for the differentially-driven antenna, (c) H-plane, (d) E-plane for the single-ended microstrip antenna.

between the simulation and experiment. It is more interesting to note that the differentially-driven microstrip antenna has much better polarization purity than that of single-ended counterpart. This is particularly remarkable in the H-plane.

The peak gain was measured with the approach of two identical antennas. The measured peak gain values at 2 GHz are 4.2 and 1.2 dBi for the differentially-driven and single-ended microstrip antennas, respectively. They are quite close to the simulated peak gain values 3.7 dBi for the differentially-driven microstrip antenna and 1.2 dBi for the single-ended microstrip antenna. It is interesting to note that the peak gain values are low, which is mainly due to the large loss tangent associated with the FR4 substrates used [14], where a single-ended microstrip antenna designed on the same FR4 substrate as we used has the measured gain of 2.3 dBi at 1.873 GHz. It is more important to note that the peak gain of the differentially-driven microstrip antenna is 3 dB (exactly from the measurements and approximately from the simulations) higher than that of the single-ended microstrip antenna. This is because what we measured were the gain values of the linearly-polarized microstrip antennas. The H-plane cross-polarization for the single-ended microstrip antenna is much higher than that of the differentially-driven microstrip antenna. Also, the differentially-driven microstrip antenna has lower matching loss than that of the single-ended microstrip antenna. Furthermore, the differentially-driven microstrip antenna has significantly suppressed the higher order TM_{20} mode; this improves the radiation efficiency of the differentially-driven microstrip antenna. Hence, the gain of the differentially-driven microstrip antenna is higher than that of the single-ended microstrip antenna.

IV. Conclusion

This paper focused on the design and experiment on differentially-driven microstrip antennas. The design procedure for differentially-driven microstrip antennas was established for the first time. The computer-aided design formulas to determine the patch dimensions and the location of the feed point for single-ended microstrip antennas were examined for differentially-driven microstrip antennas. It was found that the patch length can still be designed using the formulas for the required resonant frequency but the patch width calculated by the formula usually needs to be widen to ensure the excitation of the fundamental mode using the probe feeds. The condition that links the patch width, the locations of the probe feeds, and the excitation of the fundamental mode was given. The wideband techniques for single-ended microstrip antennas were evaluated for differentially-driven microstrip antennas. A novel H-slot was proposed for a single-layer differentially-driven rectangular microstrip antenna to improve the impedance bandwidth. The effects of imperfect differential signal conditions on the performance of differentially-driven microstrip antennas were investigated. It was found that they only degrade the polarization purity in the H-plane with an enhanced radiation of cross-polarization. Both differentially-driven and single-ended microstrip antennas were fabricated and measured. It was shown that the simulated and measured results are in acceptable agreement. More importantly, it was also shown that the differentially-driven microstrip antenna has wider impedance bandwidth of measured 4.1% and simulated 3.9% and higher gain of measured 4.2 dBi and simulated 3.7 dBi as compared with those of measured 1.9% and simulated 1.3% and gain of measured 1.2 dBi and simulated 1.2 dBi of the single-ended microstrip antenna.

Acknowledgment

The author would like to thank Dr. M. Sun, Mr. E. K. Chua, and Mr. S. H. Wi for their invaluable assistance in this work.

References

[1] Y. T. Lo, D. Solomon, and W. F. Richards, "Theory and experiment on microstrip antennas," *IEEE Trans. Antennas Propag.*, vol. 27, no. 2, pp. 137–145, 1979.

[2] A. R. Behzad, M. S. Zhong, S. B. Anand, L. Li, K. A. Carter, M. S. Kappes, T. H. Lin, T. Nguyen, D. Yuan, S. Wu, Y. C. Wong, V. Gong, and A. Rofougaran, "A 5-GHz direct-conversion CMOS transceiver utilizing automatic frequency control for the IEEE 802.11a wireless LAN standard," *IEEE J. Solid-State Circuits*, vol. 38, no. 12, pp. 2209–2220, 2003.

[3] Y. P. Zhang, Development of ICPA in LTCC for Single-Chip CMOS RF Transceivers, Tech. Rep. NTU, 2003.

[4] W. R. Deal, V. Radisic, Y. X. Qian, and T. Itoh, "Integrated-antenna push-pull power amplifiers," *IEEE Trans. Microw. Theory Tech.*, vol. 47, pp. 1418–1425, 1999.

[5] W. Wong and Y. P. Zhang, "0.18-μm CMOS push-pull power amplifier with antenna in IC package," *IEEE Microw. Wireless Comp. Lett.*, vol. 14, no. 1, pp. 13–15, 2004.

[6] P. Abele, E. Ojefors, K. B. Schad, E. Sonmez, A. Trasser, J. Konle, and H. Schumacher, "Wafer level integration of a 24 GHz differential SiGe-MMIC oscillator with a patch antenna using BCB as a dielectric layer," in *Proc. 11th GAAS Symp.*, Munich, 2003, pp. 419–422.

[7] T. Brauner, R. Vogt, and W. Bachtold, "A differential active patch antenna element for array applications," *IEEE Microw. Wireless Comp. Lett.*, vol. 13, no. 4, pp. 161–163, 2003.

[8] Y. P. Zhang and J. J. Wang, "Theory and analysis of differentially-driven microstrip antennas," *IEEE Trans. Antennas Propag.*, vol. 54, no. 4, pp. 1092–1099, 2006.

[9] W. F. Richards, Y. T. Lo, and D. D. Harrison, "An improved theory for microstrip antennas and applications," *IEEE Trans. Antennas Propag.*, vol. 29, no. 1, pp. 38–46, 1981.

[10] K. Hirasawa, *Analysis, Design, and Measurement of Small and Low-Profile Antennas*. Norwood, MA: Artech House, 1991, ch. 4.

[11] W. L. Stustzman and G. A. Thiele, *Antenna Theory and Design*. New York: Wiley, 1998, ch. 5.

[12] K. F. Tong, K. M. Luk, K. F. Lee, and R. Q. Lee, "A broad-band U-slot rectangular patch antenna on a microwave substrate ," *IEEE Trans. Antennas Propag.*, vol. 48, no. 6, pp. 954–960, 2000.

[13] S. Weigand, G. H. Huff, K. H. Pan, and J. T. Bernhard, "Analysis and design of broad-band single-layer rectangular U-slot microstrip patch antennas," *IEEE Trans. Antennas Propag.*, vol. 51, no. 3, pp. 457–468, 2003.

[14] K. L. Wong, *Compact and Broadband Microstrip Antennas*. New York: Wiley, 2002, p. 258.

Yue Ping Zhang received the B.E. and M.E. degrees from Taiyuan Polytechnic Institute and Shanxi Mining Institute of Taiyuan University of Technology, Shanxi, China, in 1982 and 1987, respectively, and the Ph.D. degree from the Chinese University of Hong Kong, Hong Kong, in 1995, all in electronic engineering.

From 1982 to 1984, he worked at Shanxi Electronic Industry Bureau, from 1990 to 1992, the University of Liverpool, Liverpool, U.K., and from 1996 to 1997, City University of Hong Kong. From 1987 to 1990, he taught at Shanxi Mining Institute and from 1997 to 1998, the University of Hong Kong. He was promoted to a Full Professor at Taiyuan University of Technology in 1996. He is now an Associate Professor and the Deputy Supervisor of Integrated Circuits and Systems Laboratories with the School of Electrical and Electronic Engineering, Nanyang Technological University, Singapore. He has broad interests in radio science and technology and published widely across seven IEEE societies. He has delivered scores of invited papers/keynote address at international scientific conferences. He has organized/chaired dozens of technical sessions of international symposia.

Dr. Zhang received the Sino-British Technical Collaboration Award in 1990 for his contribution to the advancement of subsurface radio science and technology. He received the Best Paper Award from the Second International Symposium on Communication Systems, Networks and Digital Signal Processing, held July 18–20, 2000, Bournemouth, U.K. and the Best Paper Prize from the Third IEEE International Workshop on Antenna Technology, held March 21–23, 2007, Cambridge, UK. He was awarded a William Mong Visiting Fellowship from the University of Hong Kong in 2005. He is listed in *Marquis Who's Who, Marquis Who's Who in Science and Engineering,* and *Outstanding Scientists of the 21st Century, Cambridge IBC 2000* . He serves on the Editorial Board of the *International Journal of RF and Microwave Computer-Aided Engineering* and was a Guest Editor of the Journal for the Special Issue "RF and Microwave Subsystem Modules for Wireless Communications." He also serves as an Associate Editor of the *International Journal of Microwave Science and Technology*. Furthermore, he serves on the Editorial Boards of IEEE Transactions on Microwave Theory and Techniques and the IEEE Microwave and Wireless Components Letters.